Lysozyme-Based Antibacterial Nanomotors

Melek Kiristi,[†] Virendra V. Singh,[†] Berta Esteban-Fernández de Ávila,[†] Murat Uygun, Fernando Soto, Deniz Aktaş Uygun, and Joseph Wang*

Department of Nanoengineering, University of California—San Diego, La Jolla, California 92093, United States. [†]M.K., V.V.S., and B.E.-F.d.Á. contributed equally to this work

ABSTRACT An effective and rapid bacterial killing nanotechnology strategy based on lysozyme-modified fuel-free nanomotors is demonstrated. The efficient antibacterial property of lysozyme, associated with the cleavage of glycosidic bonds of peptidoglycans present in the bacteria cell wall, has been combined with ultrasound (US)-propelled porous gold nanowire (p-AuNW) motors as biocompatible dynamic bacteria nanofighters. Coupling the antibacterial activity of the enzyme with the rapid movement of these p-AuNWs, along with the corresponding fluid dynamics, promotes enzyme—bacteria interactions and prevents surface aggregation of dead bacteria, resulting in a greatly enhanced bacteria-killing capability. The large active surface area of these nanoporous motors offers a significantly higher enzyme loading capacity compared to nonporous AuNWs, which results in a higher antimicrobial activity against Gram-positive and Gram-negative bacteria. Detailed characterization studies and control experiments provide useful insights into the underlying factors controlling the antibacterial performance of the new dynamic bacteria nanofighters. Rapid and effective killing of the Gram-positive *Micrococcus lysodeikticus* bacteria (69—84% within 1—5 min) is demonstrated.

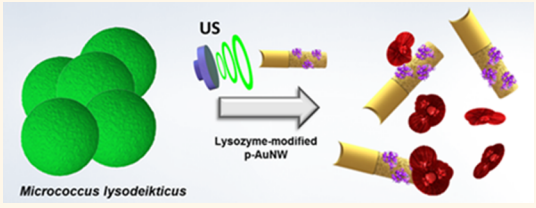

KEYWORDS: lysozyme · bacteria · nanomotors · ultrasound · biocompatibility

Bacterial outbreaks originating from human contact, food poisoning, contaminated water reservoirs, and terrorism represent a major global public health threat.[1] Antibacterial research has thus become extremely important, as traditional clinically approved antibiotic therapies are insufficient to overcome antibiotic-resistant bacterial species and microbial biofilm formations that can lead to serious life-threatening infectious diseases.[1] Current methods for the destruction of bacteria involve the use of various antimicrobial agents, such as chlorine and silver,[2] strong oxidants,[3] nonthermal plasma techniques,[4] or photocatalytic degradation.[5] Each of these methods has its drawbacks and potential risks, which prevent large-scale bacterial destructions. To address the limitations of conventional treatments and combat bacterial infections without endangering human life, major efforts are being devoted toward the development of new fast, efficient, environment-friendly, cost-efficient therapeutic routes.[6] One safe alternative relies on lysozyme-based enzymatic degradation of bacteria.[7] Lysozyme is an antibacterial glycoside-hydrolase enzyme that attacks the protective cell walls of bacteria specifically and more efficiently compared to antibiotics and quaternary ammonium compounds.[7−9] The use of free lysozyme for bacteria killing is often compromised by the limited stability and reusability of the enzyme. Different solid (polymer, nanoparticles) matrices have been introduced to increase the stability and reusability of lysozyme.[10,11] However, such lysozyme-loaded platforms are characterized by decreased enzymatic activity due to accumulation of the dead bacteria and other materials on their surface.[12]

The present work introduces a highly efficient and rapid lysozyme-based nanomotor bacteria killing system that greatly enhances the biocatalytic destruction of bacteria species. Mimicking natural motors,[13−16] man-made nanomotors have been the focus of a considerable recent attention.[16−20] The improved capabilities of modern artificial nanomotors have led to diverse biomedical[21] and environmental[22,23] applications. The motion of nanoscale reactive remediation platforms and the corresponding fluid transport can notably improve decontamination processes while

* Address correspondence to josephwang@ucsd.edu.

Received for review July 6, 2015 and accepted August 26, 2015.

Published online August 26, 2015
10.1021/acsnano.5b04142

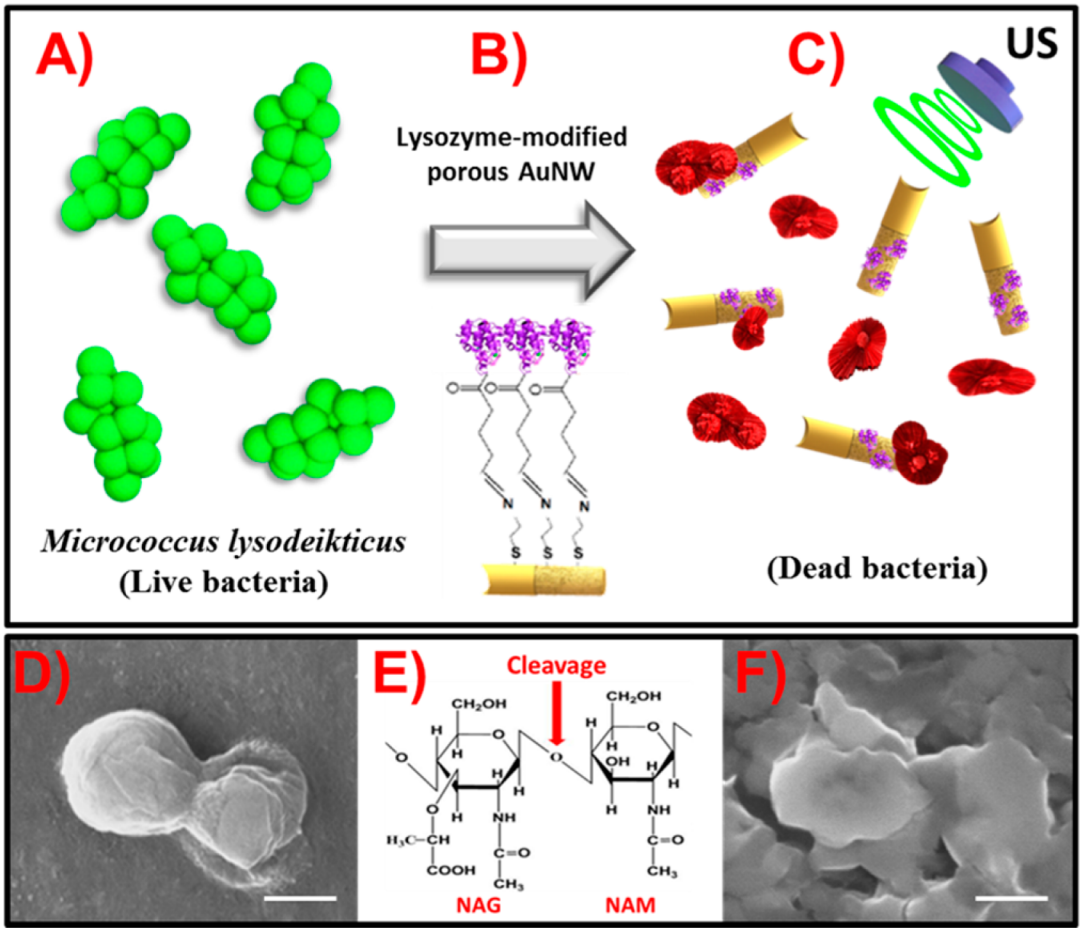

Figure 1. Nanomotors coupling the antibacterial activity of lysozyme with rapid movement toward efficient bacteria killing capability. Top: Schematic illustration of the live bacteria (*M. lysodeikticus*) (A), lysozyme immobilized on the p-AuNWs (B), and bacteria treated ("killed") by the lysozyme-modified p-AuNWs motors (C). SEM image of the live *M. lysodeikticus* bacteria (D). Structure of the bacterial cell wall: hydrolysis (cleavage) of the β-1,4 glycosidic bonds between *N*-acetylglucosamine (NAG) and *N*-acetylmuramic acid (NAM) occurs during the lysozyme treatment (E). SEM image of the dead *M. lysodeikticus* bacteria following treatment by the moving lysozyme-modified nanomotors (F). US conditions: 2.5 V and 2.67 MHz for 5 min. Scale bar: 500 nm.

reducing passivation effects. Different mechanisms have been explored for powering of these nanoscale motors, including the use of external fields or catalytic decomposition of chemical fuels.[16−19] Among these, ultrasound (US) triggered propulsion offers safety and compatibility with biological systems, without adding a chemical fuel and is of considerable interest for future *in vivo* applications.[24−26] Efficient US propulsion in biological media, and even in living cells, has been demonstrated recently.[27−29] Acoustic propulsion modes provide chemically inert nanoshuttles for transporting bioentities in an active manner. The attractive performance of US-propelled nanomotors has been improved further by controlling the design and increasing the surface area of the motor.[30] These fuel-free nanomotors have demonstrated advanced cargo-towing capabilities, collective action, propulsion in biological media, and high stability.[31] Ultrasound has been shown previously to increase the effectiveness of selected antibiotics on several bacteria[32] and to facilitate the delivery of antibacterial nanoparticles,[33] but not in connection to nanomotors.

The present fuel-free US-propelled dynamic bacterial fighter nanomotor platform offers rapid and efficient destruction of different bacterial species (Figure 1A−C). The enhanced antibacterial activity is attributed to the continuous motion of multiple lysozyme-modified nanomotors under an US field that imparts effective fluid mixing to greatly enhance the lysozyme-bacteria interactions and reduce passivation effects. Incorporating a large surface area porous gold segment to the nanomotor body increases the lysozyme loading and results in a higher antimicrobial activity against Gram-positive *M. lysodeikticus* and Gram-negative *Escherichia coli* (*E. coli*) bacteria. Spectrophotometric and fluorescence studies illustrate that the fuel-free acoustic propulsion of lysozyme-modified porous gold nanowires (p-AuNWs) results in dramatic improvements in the antibacterial efficiency compared to their static counterparts (*e.g.*, >30-fold enhancement using one min incubation). As will be illustrated in the following sections, the new bacteria nanofighter motor strategy offers an efficient and rapid bacterial killing capability (69−84% within 1−5 min), and holds considerable

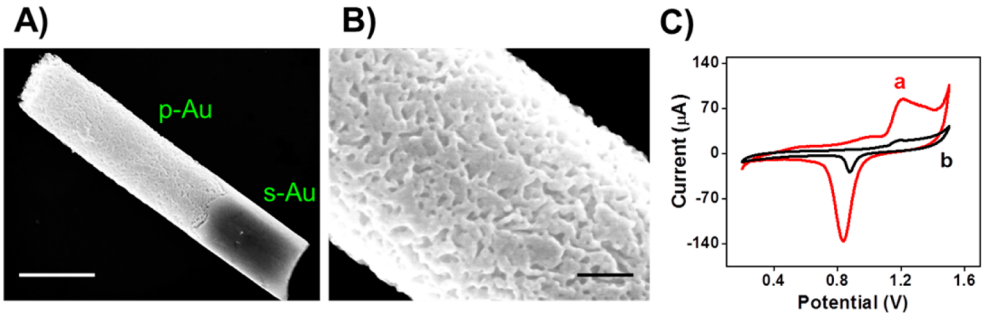

Figure 2. SEM images of porous gold nanowire (p-AuNWs), indicating the solid Au (s-Au) concave section and the porous Au (p-Au) segment (A), and of the porous segment (B). Scale bars: 300 and 50 nm, respectively. (C) Cyclic voltammograms of (a) p-AuNWs and (b) nonporous AuNWs in a N_2 saturated 0.1 M H_2SO_4 using a scan rate of 50 mV s^{-1}.

promise for diverse therapeutic, biodefense and environmental applications.

RESULTS AND DISCUSSION

Fabrication of Lysozyme-Modified p-AuNWs. The new nanomotor-based bacterial destruction strategy, illustrated in the schematic of Figure 1, is based on the strong bactericidal activity of lysozyme immobilized on US-propelled nanomotors. The driving force for this high bacterial killing efficiency is provided by continuous movement of the enzyme and convection induced by the nanomotor motion that greatly enhance bacteria killing compared to earlier protocols based on lysozyme-immobilized nanomaterials.[10−12] The immobilization of lysozyme onto the p-AuNWs was carried out by the cysteamine method (Figure 1B),[34] as detailed in the Supporting Information (Figure S1). As illustrated in Supporting Video 1, the functionalization of the p-AuNWs with lysozyme does not compromise the efficient propulsion of US-powered nanomotors. Lysozyme activity leads to hydrolytic cleavage of the β-1,4 glycosidic bonds between N-acetylmuramic acid (NAM) and N-acetylglucosamine (NAG) (Figure 1E), which are characteristic peptidoglycans of the bacteria cell wall.[35] The continuous movement of the lysozyme-modified p-AuNWs in the bacteria solution under the US field leads to enhanced contact between the enzyme and the live bacteria, resulting in accelerated bacteriolysis effect and efficient bacteria killing (Figure 1C). The scanning electron microscopy (SEM) images of Figure 1D and F illustrate the physical appearance of the *M. lysodeikticus* bacteria before and after the antibacterial treatment, respectively, and demonstrate the largely damaged bacterial cells following the nanomotor treatment.

SEM studies were carried out to examine the structural morphology of the p-AuNWs. For example, Figure 2A displays a SEM image corresponding to the complete structure of the p-AuNWs with a 2 μm length and diameter of 200 nm. The latter reflects the pore size of the membrane template used in the fabrication process. Such template electrodeposition of p-AuNWs and their modification with lysozyme are described in detail in the Experimental Section and Supporting Information (Figure S1), respectively. As shown in Figure 2A, the p-AuNWs contain two segments, a solid Au concave section and a porous Au one, with lengths of 0.5 and 1.5 μm, respectively. The concave end is essential for the acoustic propulsion mechanism through the generated pressure gradient,[36] while the porous one ensures high enzyme loading. Figure 2B shows the detail of the porous segment of the p-AuNW, illustrating its large surface area toward high lysozyme-loading capacity. Cyclic voltammetry was used to characterize and compare the electrochemically active surface area (ECSA) of the p-AuNW and nonporous AuNW motors (Figure 2C). The ECSA measurements were performed in 0.1 M H_2SO_4 solution by scanning the potential over the 0.2 to 1.5 V range (*vs* Ag/AgCl). The ECSAs were calculated by integrating the charge associated with the reduction of the gold oxide peaks using GPES software for the Au oxide reduction. The resulting ECSA values for the porous and nonporous AuNWs were 377 and 42 μC, respectively, indicating that the porous gold structure has a nearly 10-fold larger area compared to the nonporous gold surface. As will be illustrated below, such high surface area and corresponding high lysozyme loading greatly enhances the bactericidal capacity of the motors.

Key factors controlling the antibacterial activity of the functionalized nanomotors have been elucidated toward optimizing the bacteria killing operation of the modified nanomotors. Figure 3A examines the influence of the treatment time upon the efficiency using times ranging from 30 s to 5 min. The bacteria killing efficiency of the p-AuNWs increases from 32% to 84% over this time scale (a). In contrast, the static counterparts lead to significantly lower efficiencies ranging from 2% at 30 s to 9% at 5 min. Note that the nanomotors yield dramatic improvements in the antibacterial efficiency using short treatment times (*e.g.*, >30-fold using one min). In order to compare further the efficiency of nanomotors with their static counterpart, the treatment time using the static p-AuNWs was extended to 40 min, leading to a 60% bacteria killing

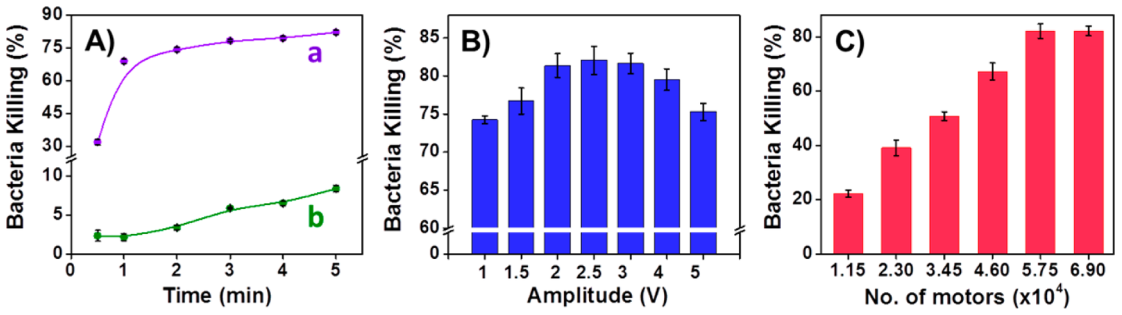

Figure 3. Effect of relevant parameters upon the *M. lysodeikticus* bacteria killing capability of US-driven lysozyme-modified p-AuNWs. Effect of the (A) treatment time with (a) and without (b) the US field. Effect of the (B) US voltage and (C) number of nanomotors upon the bacteria killing efficiency. US conditions: 2.5 V, 2.67 MHz for 5 min (except A) and using 5.75 × 10^4 motors (except C).

efficiency (compared to 84% within 5 min using the nanomotors). Only a slight increase in the bacteria killing efficiency up to 95% was obtained upon extending the treatment time to 15 min (not shown), due to the saturation of the enzymatic activity at higher treatment times. Subsequent absorbance measurements (without US and lysozyme), over an additional 15 min period, indicated similar bacteria concentrations, *i.e.*, negligible regrowth of the bacteria.

Another parameter studied was the US amplitude used for controlling the speed of the p-AuNWs. Figure 3B (and Supporting Video 1) evaluate the influence of the US voltage and demonstrates that an amplitude of 2.5 V offers the optimum condition, with 82% killing efficiency within 5 min. These data indicate that the bactericidal capacity increases gradually from 74 to 82% between 1.0 and 2.5 V, and decreases back to 74% upon raising the amplitude to 5 V. Such a trend indicates that the 2.5 V value provides a trade-off between higher motor speeds and reduced enzymatic activity (due to thermal inactivation at high voltages).[37] While ultrasonic waves at room temperature and pressure hardly inactivate lysozyme,[37] such inactivation depends on the US parameters. High US voltages lead to collapsing cavitation bubbles that raise the local temperature. The number of modified nanomotors in the treated media is another important parameter. Figure 3C illustrates that the bacteria killing capacity increases from 21% using 1.15 × 10^4 p-AuNWs to 82% at 5.75 × 10^4 nanomotors. The latter value was employed in all further bacteria killing studies. Overall, the data of Figure 3 indicate that the antibacterial activity can be controlled by tuning the parameters of the lysozyme nanomotor strategy. The effect of temperature upon the activity of the free and immobilized lysozyme was investigated. The results, shown in Figure S2, indicate that the activity increases gradually by ~30% upon raising the temperature from 25 to 45 °C, and decreases fast thereafter, reflecting the temperature dependence of lysozyme and its thermal denaturation. The optimal lysozyme activity depends on several experimental conditions, such the source of lysozyme, pH, substrate and temperature.[38−40]

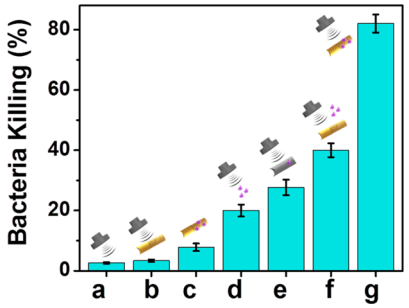

Figure 4. US-driven lysozyme-immobilized p-AuNW motors for killing bacteria along with different control experiments. Bacteria killing efficiency, estimated by UV−vis spectroscopy, using (a) only US without AuNWs, (b) nonfunctionalized p-AuNWs, (c) static lysozyme-modified p-AuNWs (no US), (d) free-lysozyme, (e) lysozyme-modified nonporous AuNWs, (f) free-lysozyme and p-AuNWs, and (g) lysozyme-modified p-AuNWs. US conditions (except C): 2.5 V, 2.67 MHz for 5 min; 2 mg/mL of bacteria along with 5.75 × 10^4 motors; amount of free enzyme (d, f), 0.19 mg/100 μL.

Under the applied US treatment, the solution temperature raises to ~40 °C which is nearly optimal for the lysozyme activity.

Lysozyme-Modified p-AuNWs: Control Experiments. Following the optimization studies, we carried out a series of different control experiments aimed at gaining further insights into the new protocol, elucidating the role of the different components and processes involved, and at demonstrating the distinct advantages of the bacteria-killing nanomotor strategy. These control experiments involved spectrophotometric optical density measurements of the *M. lysodeikticus* and *E. coli* at 450 and 600 nm, respectively. Figure 4 shows the spectrophotometrically estimated bacteria killing capability using various control systems under optimal conditions. Initial control experiments using the US alone and US with unmodified wires (Figure 4a and b, respectively) indicate negligible (~3%) bacteria killing efficiency. Apparently, such US conditions do not disrupt the cell membranes. Similarly, Figure 4c illustrates that the use of the functionalized p-AuNW without US results in a low bacteria killing efficiency (7%) over the same (5 min) incubation time. The US-driven modified p-AuNW motors resulted in a nearly 12-fold higher

antibacterial activity compared to static counterparts (81% compared with 7%) (Figure 4g *vs* c). The antibacterial activity of free lysozyme under the US field was examined and resulted in a 20% of bacteria killing efficiency (Figure 4d). Such efficiency is over 4 times lower compared to the activity observed with the lysozyme-modified-p-AuNWs (Figure 4g *vs* d), reflecting the key role of moving the immobilized enzyme throughout the bacteria solution, and indicates that the covalently bound enzyme is not desorbing from the wires during the US-driven motion. The US-powered lysozyme p-AuNW motors offer ~3-fold enhanced killing efficiency compared to their nonporous counterparts (Figure 4g *vs* e). Such improvement due to the porous structure is lower than that expected (based on the ECSA data of Figure 2C), which can be explained by the limited accessibility of the enzyme to the entire gold surface of the motor.[10] Apparently, the surface loading of the enzyme does not follow directly the increased area of the porous motor, as the interior of the porous wire may not be fully accessible during the immobilization. Another control experiment involving both the free enzyme and the unmodified wires under the optimal US conditions led to a 40% of bacterial killing capacity (Figure 4f). While the movement of the nanowires in the enzyme solution resulted enhanced fluid mixing which leads to increased enzyme-bacteria interactions compared to free-enzyme alone (Figure 4d *vs* f). However, the extent of these interactions is significantly lower compared to the lysozyme p-AuNW motors (Figure 4f *vs* g). The latter reflects the directional collisions of the enzyme-modified AuNWs with the bacteria wall. Overall, the control experiments of Figure 4 demonstrate that the US propulsion of the lysozyme-modified AuNWs greatly promotes their interaction with the bacteria suspension and that the porous surface feature increases the enzyme-loading capacity.

Figure 5 shows SEM images of *M. lysodeikticus* before (A) and after (B) 5 min treatment with US-driven lysozyme-modified p-AuNWs. These images clearly illustrate the dramatic change of the morphology and structure of the bacteria cell wall and disappearance of cellular integrity in the presence of the US-propelled antibacterial nanomotors, as expected from the biocatalytic hydrolysis of glycosidic linkages. The wrinkled cell wall may reflect leakage of cytoplasmic content outside the bacterial cell.[41]

Additional fluorescence imaging viability studies were performed to support the early UV−vis spectrophotometric data and evaluate further the nanomotors-based killing efficiency for different (Gram-positive and negative) bacteria species. Syto-9 dye was used to label all the population of bacteria cells (live and dead *M. lysodeikticus*), while the propidium iodide dye was used to label dead *M. lysodeikticus*, as propidium iodide penetrates only the damaged cells. These dyes thus allowed estimate of the number of viable and nonviable

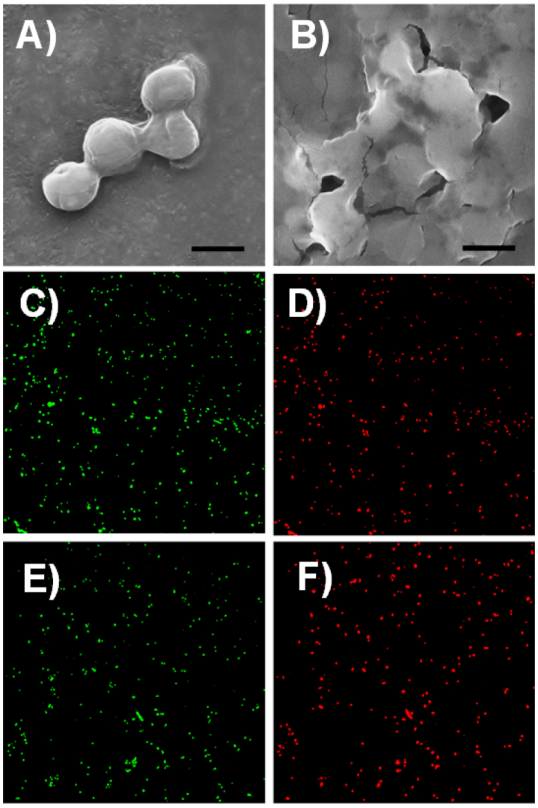

Figure 5. Lysozyme-modified nanomotor-accelerated destruction of different bacterial species. SEM images of the *M. lysodeikticus* bacteria (A) before and (B) after US treatment with lysozyme-modified nanomotors. Fluorescence images of (C) total *M. lysodeikticus* present in the solution and of (D) dead *M. lysodeikticus* after US treatment with lysozyme-modified nanomotors; similar images of (E) total *E. coli* present and (F) dead *E. coli* after the US nanomotor treatment. Scale bar: 1 μm. US conditions: 5 min using 2.5 V and 2.67 MHz, using 5.75 $\times$ 10^4 motors.

cells in connection to a program ImageJ. Figure 5C and D show fluorescence images of total *M. lysodeikticus* (in green color) and of dead *M. lysodeikticus* (in red color). Based on program ImageJ the percentage bacteria killing was found to be 84% in 5 min, which is in agreement with UV−visible data. Similar UV−visible and fluorescence studies were performed to examine the killing of the Gram-negative *E. coli* bacteria. The UV−visible data (not shown) was found to be in agreement with the fluorescence data (Figure 5E, F), illustrating a 70% bacterial killing efficiency for *E. coli* samples. The different killing efficiencies of the bacteria nanofighter motors obtained against *M. lysodeikticus* and *E. coli* reflects the higher antimicrobial efficacy of lysozyme toward Gram-positive bacteria, possibly due to the difference in the cell wall structure of the bacteria species.[12] The ability to kill both bacteria species with high efficiency is important as Gram-negative infections are becoming increasingly difficult to treat.[1] Overall, Figure 5 demonstrates the potential applicability of the new antibacterial nanomotor fighters for effective bacteria killing in a fast and environmentally friendly manner.

CONCLUSIONS

The motivation of this study was to demonstrate a highly efficient and rapid bacteria-killing strategy based on the coupling the antibacterial activity of the lysozyme with the continuous movement of fuel-free nanowire motors. To our knowledge, this is the first report documenting that nanomotors can inactivate bacteria within a few minutes. The motion of lysozyme-loaded US-driven porous nanomotors in bacterial-contaminated samples, along with the corresponding fluid mixing, greatly enhances the lysozyme-bacteria interactions and bacterial killing capability, as was demonstrated using *M. lysodeikticus* and *E. coli* bacterial models. Dramatic improvements in the antibacterial efficiency was achieved compared to the corresponding static functionalized nanowires (*e.g.*, >30-fold enhancement using one min incubation). Various control experiments have demonstrated the distinct advantages of the new dynamic bacterial nanofighters, shed useful insights into the factors affecting the performance of the new nanomotor bacteria killing system and led to optimization of the new dynamic antibacterial nanotechnology strategy. Swarms of US-powered micromotors[31] could be used for accelerating the bacterial killing using large sample volumes or contaminated areas, while guidance of the motors could be achieved by adding a magnetic segment.[36] The favorable capabilities of these fuel-free US-driven functionalized antibacterial nanoswimmers along with the biocompatibility of acoustic waves make them extremely attractive for combating infectious diseases while offering defense against bacterial infections in connection to diverse healthcare, biodefense, and food or water disinfection applications. The biocompatibility of the ultrasound operation, of nano/microscale machines[42] and of the lysozyme, make the new antibacterial nanomotors very attractive not only to diverse *in vitro* applications, but also for *in vivo* biomedical ones.

EXPERIMENTAL SECTION

Materials and Instruments. Anodic alumina membranes (AAO) with a specified pore size of 200 nm and thickness of 60 μm were purchased from Whatman (catalog no. 6809-6022; Maidstone, U.K.). The gold and silver plating solutions (Orotemp 24 RTU RACK, and 1025 RTU @ 4.5 Troy/gallon) were obtained from Technic Inc. (Anaheim, CA). Lysozyme (from chicken egg white), *M. lysodeikticus* and *E. coli* bacterial cells, and cysteamine hydrochloride were purchased from Sigma-Aldrich (St. Louis, MO). All chemicals were analytical-grade reagents and were used as received without any further purification. Experiments were carried out at room temperature (21 °C).

All controlled-potential experiments were performed with a CHI 621A potentiostat (CH Instruments, Austin, TX). The ECSA characterization was carried out using a μ-Autolab type II (Eco Chemie, Utrecht, Netherlands) system, operating with GPES software, along with a conventional three-electrode electrochemical cell.

Template Electrosynthesis of p-AuNWs. Nanoporous gold structures were commonly prepared on two-dimensional flat AAO substrates through template electrodeposition of a single-phase Au−Ag alloy followed by etching of the less noble silver component, similar to a previous protocol.[12] To obtain a working electrode the branched side of the AAO membrane was sputtered with a 200 nm thick Ag film. The membrane was then placed in a Teflon plating cell, with aluminum foil serving as a contact. A sacrificial Ag layer was electrodeposited for a total charge of 3 C using a commercial Ag plating solution at a potential of −1.0 V (*vs* Ag/AgCl (1 M KCl)), in connection to a Pt wire counter electrode. Subsequently, an Au segment was electroplated from a commercial Au plating solution using a potential of −1.0 V and a total charge of 1 C. Finally, Au−Ag alloy was electrodeposited from a mixture of commercial gold and silver plating solutions (Au/Ag ratio of 7/3) at a potential of −1.1 V for 1.7 C. The Au/Ag alloy segment was dealloyed using a 35% HNO_3 solution (EMD Millipore, MA) in the plating cell for 10 min. The membranes were then removed from the plating cell and rinsed thoroughly with ultrapure water. The sacrificial Ag layer was removed using a cotton tip applicator soaked in 35% HNO_3 solution. The AAO membrane template was dissolved in a 3 M NaOH solution for 30 min to release the nanowires. The nanowires were then washed repeatedly with deionized water until a neutral pH was obtained. Control nonporous AuNWs were prepared in the same manner, as described above, except that both Au segments were electroplated for 1.2 C.

AuNW Modification and Lysozyme Immobilization. Immobilization of lysozyme onto p-AuNW was carried out by using the cysteamine method,[34] as illustrated in Figure S1. Briefly, 1.0 mg/100 μL of cysteamine solution (in pH 7.4 phosphate buffer, 100 mM) was mixed with 100 μL of nanowire suspension and incubated at room temperature for 1 h. Cysteamine modified nanowires were then washed with phosphate buffer, in order to remove unreacted cysteamine. These functionalized nanowires then were further modified with glutaraldehyde by overnight incubation with a glutaraldehyde solution (1%, in pH 7.4 phosphate buffer; 100 mM). After modification, nanowires (5.75×10^4 motors/100 μL) were mixed with 500 μL of lysozyme solution (5 mg/mL) and incubated under shaking for 3 h. The amount of lysozyme attached to the nanowires was estimated by spectrophotometric protein measurement at 280 nm for the initial and final lysozyme concentrations of the immobilization medium. The lysozyme modified nanowires were washed with phosphate buffer and stored at 4 °C until use.

Activity of Lysozyme and Determination of the Bacteria Killing Capability. The activity of lysozyme was estimated spectrophotometrically (Shimadzu UV-2450, Japan). For this aim, a suspension of bacteria cells was prepared by dissolving 9.0 g of *M. lysodeikticus* in 30.0 mL of carbonate buffer (pH 9.0; 100 mM). The enzymatic reaction was started by mixing 580 μL of cell suspension and 20 μL of lysozyme solution. Cell lysis was monitored optically at 450 nm for 5 min. One unit of lysozyme activity is defined as a decrease of 0.001 unit of absorbance at 450 nm by using carbonate buffer (pH 9.0; 100 mM) at 25 °C.

Antibacterial activity of lysozyme-immobilized p-AuNWs was examined by using US setup in connection to *M. lysodeikticus* (0.3 mg/mL) and *E. coli* (1×10^8 cells mL^{-1}). To check the efficiency of US-driven lysozyme-immobilized p-AuNWs and its static counterparts, *E. coli* and *M. lysodeikticus* bacteria were taken into separate US holders in 25 μL aqueous solutions containing 5.75×10^4 motors. The reaction mixture was subjected to an US amplitude of 2.5 V, and frequency of 2.67 MHz for 5 min and the bacteria-killing capacity was studied by using two methods. The first method was based on spectrophotometric turbidity measurements at 450 nm for *M. lysodeikticus* and 600 nm for *E. coli*. Briefly, destroyed bacteria were removed from the US holder and mixed with 475 μL of carbonate buffer (pH 9.0, 100 mM) and the optical densities of samples were recorded using the corresponding wavelength. Antibacterial capacities of the lysozyme-attached nanowires were calculated by using blank sample, which contains the same amount of bacteria but without enzyme.

The second method involved fluorescence measurements. For this, following the 5 min US incubations, the nanomotors were precipitated at 500 rpm for 1 min, and the supernatant (containing viable and nonviable bacteria cells) was centrifuged again at 14 000 rpm to make a bacterial pellet. The pellet was resuspended in 100 μL of a solution of Syto-9 dye and propidium iodide dye previously dissolved in water following specifications of the L13152LIVE/DEADBac Light bacterial viability kit provider. Eppendorf vials were covered with aluminum foil and gently mixed for 20 min. A washing step was performed to remove the unreacted dye. Additionally, the vials were centrifuged at 14 000 rpm for 10 min and the pellet was resuspended in 100 μL of water for counting. Fluorescent pictures of 2 μL drops were obtained and the number of viable and nonviable cells was estimated using the program ImageJ.

Effect of the Temperature on the Enzyme Activity. The effect of the temperature on the lysozyme activity was studied by varying temperature from 25 to 65 °C. Briefly, 580 μL of the substrate solution (*M. lysodeikticus*) was incubated at the desired temperature for 10 min, and then mixed with 20 μL of enzyme solution (free lysozyme and immobilized lysozyme at the same concentration level) for a 5 min incubation period. Bacteria cell lysis was monitored spectrophotometrically following the protocol described earlier (leading to the results summarized in Figure S2).

Ultrasound Propulsion. The experiments were realized in an acoustic resonator setup, consisted of a piezoelectric transducer (Ferroperm PZ26 disk 10 mm diameter, 0.5 mm thickness), attached by conductive epoxy glue to the bottom center of a steel plate (50 mm × 50 mm × 0.94 mm); the top center of the steel plate has a sample reservoir (5 mm wide, 249 μm deep) made with a kapton tape protective layer. A glass slide was used to cover the reservoir, for ultrasound reflection and to protect the sample. The continuous ultrasound sine wave was applied via a piezoelectric transducer, through an Agilent 15 MHz arbitrary waveform generator, connected to a homemade power amplifier. The applied sine waveform had a frequency of 2.66 MHz and voltage amplitude, which varied from 1 to 5 V, to modulate the intensity of the acoustic waves.

Conflict of Interest: The authors declare no competing financial interest.

Supporting Information Available: The Supporting Information is available free of charge on the ACS Publications website at DOI: 10.1021/acsnano.5b04142.

Schematic illustration of the immobilization of lysozyme onto porous Au nanowires by cysteamine method; temperature effect on enzyme activity (PDF)

Motion of the lysozyme-modified ultrasound-powered p-AuNWs (AVI)

Acknowledgment. This work was supported by the Defense Threat Reduction Agency Joint Science and Technology Office for Chemical and Biological Defense (Grants Nos. HDTRA1-13-1-0002 and HDTRA1-14-1-0064). M.K., M.U., and D.A.U. acknowledge fellowships from The Scientific and Technological Research Council of Turkey (TUBITAK). F.S. acknowledges the UC MEXUS-CONACYT Doctoral Fellow.

REFERENCES AND NOTES

1. Scanlon, T. C.; Teneback, C. C.; Gill, A.; Bement, J. L.; Weiner, J. A.; Lamppa, J. W.; Leclair, L. W.; Griswold, K. E. Enhanced Antimicrobial Activity of Engineered Human Lysozyme. *ACS Chem. Biol.* **2010**, *5*, 809–818.
2. Kim, J.; Pitts, B.; Stewart, P. S.; Camper, A.; Yoon, J. Comparison of the Antimicrobial Effects of Chlorine, Silver Ion, and Tobramycin on Biofilm. *Antimicrob. Agents Chemother.* **2008**, *52*, 1446–1453.
3. Dodd, M. C.; Kohler, H-P.E.; von Gunten, U. Oxidation of Antibacterial Compounds by Ozone and Hydroxyl Radical: Elimination of Biological Activity during Aqueous Ozonation Processes. *Environ. Sci. Technol.* **2009**, *43*, 2498–2504.
4. Moreau, M.; Orange, N.; Feuilloley, M. G. J. Non-thermal Plasma Technologies: New tools for Bio-decontamination. *Biotechnol. Adv.* **2008**, *26*, 610–617.
5. Xia, D.; Shen, Z.; Huang, G.; Wang, W.; Yu, J. C.; Wong, P. K. Red Phosphorus: An Earth-Abundant Elemental Photocatalyst for "Green" Bacterial Inactivation under Visible Light. *Environ. Sci. Technol.* **2015**, *49*, 6264–6273.
6. Thallinger, B.; Prasetyo, E. N.; Nyanhongo, G. S.; Guebitz, G. M. Antimicrobial enzymes: an emerging strategy to fight microbes and microbial biofilms. *Biotechnol. J.* **2013**, *8*, 97–109.
7. Yuan, S.; Wan, D.; Liang, B.; Pehkonen, S. O.; Ting, Y. P.; Neoh, K. G.; Kang, E. T. Lysozyme-Coupled Poly(poly(ethylene glycol) methacrylate)−Stainless Steel Hybrids and Their Antifouling and Antibacterial Surfaces. *Langmuir* **2011**, *27*, 2761–2774.
8. Banerjee, I.; Pangule, R. C.; Kane, R. S. Antifouling Coatings: Recent Developments in the Design of Surfaces That Prevent Fouling by Proteins, Bacteria, and Marine Organisms. *Adv. Mater.* **2011**, *23*, 690–718.
9. Guascito, M. R.; Chirizzi, D.; Malitesta, C.; Giotta, L.; Mastrogiacomo, D.; Valli, L.; Stabili, L. Development and characterization of a novel bioactive polymer with antibacterial and lysozyme-like activity. *Biopolymers* **2014**, *101*, 461–470.
10. Qian, X.; Levenstein, A.; Gagner, J. E.; Dordick, J. S.; Siegel, R. W. Protein Immobilization in Hollow Nanostructures and Investigation of the Adsorbed Protein Behavior. *Langmuir* **2014**, *30*, 1295–1303.
11. Tripathy, N.; Ahmad, R.; Bang, S. H.; Min, J.; Hahn, Y.-B. Tailored lysozyme−ZnO Nanoparticle Conjugates as Nanoantibiotics. *Chem. Commun.* **2014**, *50*, 9298–9301.
12. Yu, Q.; Ista, L. K.; Lopez, G. P. Nanopatterned Antimicrobial Enzymatic Surfaces Combining Biocidal and Fouling Release Properties. *Nanoscale* **2014**, *6*, 4750–4757.
13. Schliwa, M.; Woehlke, G. Molecular motors. *Nature* **2003**, *422*, 759–765.
14. Wang, J. Can Man-Made Nanomachines Compete with Nature Biomotors? *ACS Nano* **2009**, *3*, 4–9.
15. Ahmad, Z.; Cox, J. L. ATP Synthase: The Right Size Base Model for Nanomotors in Nanomedicine. *Sci. World J.* **2014**, *2014*, 1–10.
16. Wang, J. *Nanomachines: Fundamentals and Applications*; Wiley-VCH; Weinheim, Germany, 2013.
17. Guix, M.; Mayorga-Martinez, C. C.; Merkoçi, A. Nano/Micromotors in (Bio)chemical Science Applications. *Chem. Rev.* **2014**, *114*, 6285–6322.
18. Sanchez, S.; Soler, L.; Katuri, J. Chemically Powered Micro- and Nanomotors. *Angew. Chem., Int. Ed.* **2015**, *54*, 1414–1444.
19. Paxton, W. F.; Sundararajan, S.; Mallouk, T. E.; Sen, A. Chemical Locomotion. *Angew. Chem., Int. Ed.* **2006**, *45*, 5420–5429.
20. Pumera, M. Electrochemically Powered Self-propelled Electrophoretic Nanosubmarines. *Nanoscale* **2010**, *2*, 1643–1649.
21. Wang, J.; Gao, W. Nano/Microscale Motors: Biomedical Opportunities and Challenges. *ACS Nano* **2012**, *6*, 5745–5751.
22. Gao, W.; Wang, J. The Environmental Impact of Micro/Nanomachines: A Review. *ACS Nano* **2014**, *8*, 3170–3180.
23. Soler, L.; Sanchez, S. Catalytic Nanomotors for Environmental Monitoring and Water Remediation. *Nanoscale* **2014**, *6*, 7175–7182.
24. Kagan, D.; Benchimol, M. J.; Claussen, J. C.; Chuluun-Erdene, E.; Esener, S.; Wang, J. Acoustic Droplet Vaporization and Propulsion of Perfluorocarbon-Loaded Microbullets for Targeted Tissue Penetration and Deformation. *Angew. Chem.* **2012**, *124*, 7637–7640.
25. Wang, W.; Castro, L. A.; Hoyos, M.; Mallouk, T. E. Autonomous Motion of Metallic Microrods Propelled by Ultrasound. *ACS Nano* **2012**, *6*, 6122–6132.
26. Rao, K. J.; Li, F.; Meng, L.; Zheng, H.; Cai, F.; Wang, W. A Force to Be Reckoned With: A Review of Synthetic Microswimmers Powered by Ultrasound. *Small* **2015**, *11*, 2836.

27. Wang, W.; Li, S.; Mair, L.; Ahmed, S.; Huang, T. J.; Mallouk, T. E. Acoustic Propulsion of Nanorod Motors Inside Living Cells. *Angew. Chem.* **2014**, *126*, 3265–3268.
28. Wu, Z.; Li, T.; Gao, W.; Xu, T.; Jurado-Sánchez, B.; Li, J.; Gao, W.; He, Q.; Zhang, L.; Wang, J. Cell-Membrane-Coated Synthetic Nanomotors for Effective Biodetoxification. *Adv. Funct. Materials* **2015**, *25*, 3881.
29. Esteban-Fernandez de Avila, B.; Martin, A.; Soto, F.; Lopez-Ramirez, M. A.; Campuzano, S.; Vasquez-Machado, G. M.; Gao, W.; Zhang, L.; Wang, J. Single Cell Real-Time miRNAs Sensing Based on Nanomotors. *ACS Nano* **2015**, *9*, 6756–6764.
30. Garcia-Gradilla, V.; Sattayasamitsathit, S.; Soto, F.; Kuralay, F.; Yardimci, C.; Wiitala, D.; Galarnyk, M.; Wang, J. Ultrasound-Propelled Nanoporous Gold Wire for Efficient Drug Loading and Release. *Small* **2014**, *10*, 4154–4159.
31. Xu, T.; Soto, F.; Gao, W.; Dong, R.; Garcia-Gradilla, V.; Magana, E.; Zhang, X.; Wang, W. Reversible Swarming and Separation of Self-Propelled Chemically Powered Nanomotors under Acoustic Fields. *J. Am. Chem. Soc.* **2015**, *137*, 2163–2166.
32. Rediske, A. M.; Hymas, W. C.; Wilkinson, R.; Pitt, W. G. Ultrasonic Enhancement of Antibiotic Action on Several Species of Bacteria. *J. Gen. Appl. Microbiol.* **1998**, *44*, 283–288.
33. Shrestha, A.; Fong, S. W.; Khoo, B. C.; Kishen, A. Delivery of Antibacterial Nanoparticles into Dentinal Tubules using High-intensity Focused Ultrasound. *Journal of Endodontics* **2009**, *35*, 1028–1033.
34. Liu, Z.-M.; Yang, Y.; Wang, H.; Liu, Y.-L.; Shen, G.-L.; Yu, R.-Q. A Hydrogen Peroxide Biosensor based on nano-Au/PAMAM Dendrimer/Cystamine Modified Gold Electrode. *Sens. Actuators, B* **2005**, *106*, 394–400.
35. Strominger, J. L.; Tipper, D. J. Structure of Bacterial Cell Walls: the Lysozyme Substrate. In *Lysozyme*; Osserman, F., Canfield, R. E., Beychok, S., Eds.; Academic Press: New York, 1974; Ch. 16.
36. Garcia-Gradilla, V.; Orozco, J.; Sattayasamitsathit, S.; Soto, F.; Kuralay, F.; Pourazary, A.; Katzenberg, A.; Gao, W.; Shen, Y.; Wang, J. Functionalized Ultrasound-Propelled Magnetically Guided Nanomotors: Toward Practical Biomedical Applications. *ACS Nano* **2013**, *7*, 9232–9240.
37. Manas, P.; Munoz, B.; Sanz, D.; Condon, S. Inactivation of Lysozyme by Ultrasonic Waves under Pressure at Different Temperatures. *Enzyme Microb. Technol.* **2006**, *39*, 1177–1182.
38. Chang, Y. K.; Chu, L. A Simple Method for Cell Disruption by Immobilization of Lysozyme on the Extrudate-Shaped NaY Zeolite. *Biochem. Eng. J.* **2007**, *35*, 37–47.
39. Noritomi, H.; Ishiyama, R.; Kai, R.; Iwai, D.; Tanaka, M.; Kato, S. Immobilization of Lysozyme on Biomass Charcoal Powder Derived from Plant Biomass Wastes. *J. Biomater. Nanobiotechnol.* **2012**, *3*, 446–451.
40. Park, J. M.; Kim, M.; Park, H. S.; Jang, A.; Min, J.; Kim, Y. H. Immobilization of Lysozyme-CLEA onto Electrospun Chitosan Nanofiber for Effective Antibacterial Applications. *Int. J. Biol. Macromol.* **2013**, *54*, 37–43.
41. Matsumura, Y.; Yoshikata, K.; Kunisaki, S.; Tetsuaki-Tsuchido, T. Mode of Bactericidal Action of Silver Zeolite and Its Comparison with that of Silver Nitrate. *Appl. Environ. Microbiol.* **2003**, *69*, 4278–4281.
42. Khim Chng, E. L.; Zhao, G.; Pumera, M. Towards Biocompatible Nano/Microscale Machines: Self-Propelled Catalytic Nanomotors not Exhibiting Acute Toxicity. *Nanoscale* **2014**, *6*, 2119–2124.